Air Pollution in China: Mapping of Concentrations and Sources

Robert A. Rohde[1]*, **Richard A. Muller**[1,2]*

1 Berkeley Earth, Berkeley, California, United States of America, 2 Department of Physics, University of California, Berkeley, California, United States of America

* robert@berkeleyearth.org (RAR); rich@berkeleyearth.org (RAM)

Abstract

China has recently made available hourly air pollution data from over 1500 sites, including airborne particulate matter (PM), SO_2, NO_2, and O_3. We apply Kriging interpolation to four months of data to derive pollution maps for eastern China. Consistent with prior findings, the greatest pollution occurs in the east, but significant levels are widespread across northern and central China and are not limited to major cities or geologic basins. Sources of pollution are widespread, but are particularly intense in a northeast corridor that extends from near Shanghai to north of Beijing. During our analysis period, 92% of the population of China experienced >120 hours of unhealthy air (US EPA standard), and 38% experienced average concentrations that were unhealthy. China's population-weighted average exposure to $PM_{2.5}$ was 52 μg/m^3. The observed air pollution is calculated to contribute to 1.6 million deaths/year in China [0.7–2.2 million deaths/year at 95% confidence], roughly 17% of all deaths in China.

Introduction

Air pollution is a problem for much of the developing world and is believed to kill more people worldwide than AIDS, malaria, breast cancer, or tuberculosis [1–4]. Airborne particulate matter (PM) is especially detrimental to health [5–8], and has previously been estimated to cause between 3 and 7 million deaths every year, primarily by creating or worsening cardiorespiratory disease [2–4,6,7]. Particulate sources include electric power plants, industrial facilities, automobiles, biomass burning, and fossil fuels used in homes and factories for heating. In China, air pollution was previously estimated to contribute to 1.2 to 2 million deaths annually [2–4].

In 2012, China adopted the Ambient Air Quality Standard [9], and began development of a national Air Reporting System that now includes 945 sites in 190 cities. These automated stations report hourly via the internet, and focus on six pollutants: particulate matter < 2.5 microns ($PM_{2.5}$), particulate matter < 10 microns (PM_{10}), sulfur dioxide (SO_2), nitrogen dioxide (NO_2), ozone (O_3), and carbon monoxide (CO). Provincial governments perform air quality monitoring at 600 additional locations that are not yet integrated into the national system. Previous studies of regional scale air pollution have generally relied on satellite data [10,11] or modeling [12,13], but the high density of hourly data in China now allows regional patterns to be constructed directly from ground observations.

Materials and Methods

Though China deserves praise for its monitoring system and transparent communication, most archived observations are not publicly available. To compensate, real-time data was downloaded every hour during a four month interval from April 5, 2014 to August 5, 2014. Due to download restrictions on the official Chinese air quality reporting system, two different third-party sources were used: PM25.in and AQICN.org. PM25.in is a direct mirror of data from the 945 stations in China's national network, while AQICN.org is the world's largest aggregator of real-time air quality data and included many additional sites in China and surrounding areas. Nearly all of the additional data from within China originates from stations operated by provincial environmental agencies that have not yet been incorporated in China's national network.

Consistency, quality control, and validation checks were applied to the raw data prior to further analysis in order to reduce the impact of outliers, badly calibrated instruments, and other problems. The most common quality problem was associated with stuck instruments that implausibly reported the same concentration continuously for many hours. A regional consistency check was also applied to verify that each station was reporting data similar to its neighboring stations. Approximately 8% of the data was removed as a result of the quality control review. Further details are described in the supplemental material (S1 Text).

As little monitoring is conducted in western China (Fig 1); we will focus on China east of 95° E, which includes 97% of the population. After removing stations with a high percentage of missing values or with other quality control problems, this study used 880 national network sites, 640 other sites in China and Taiwan, and 236 sites in other countries within 500 km of China (mostly South Korea). The air quality network is skewed towards urban areas, often with several sites per city and fewer, if any, in rural areas. For the n-th site, we use $p_n(t)$ to denote the pollutant concentration time series and $\bar{p}_n$ to denote the mean pollutant concentration.
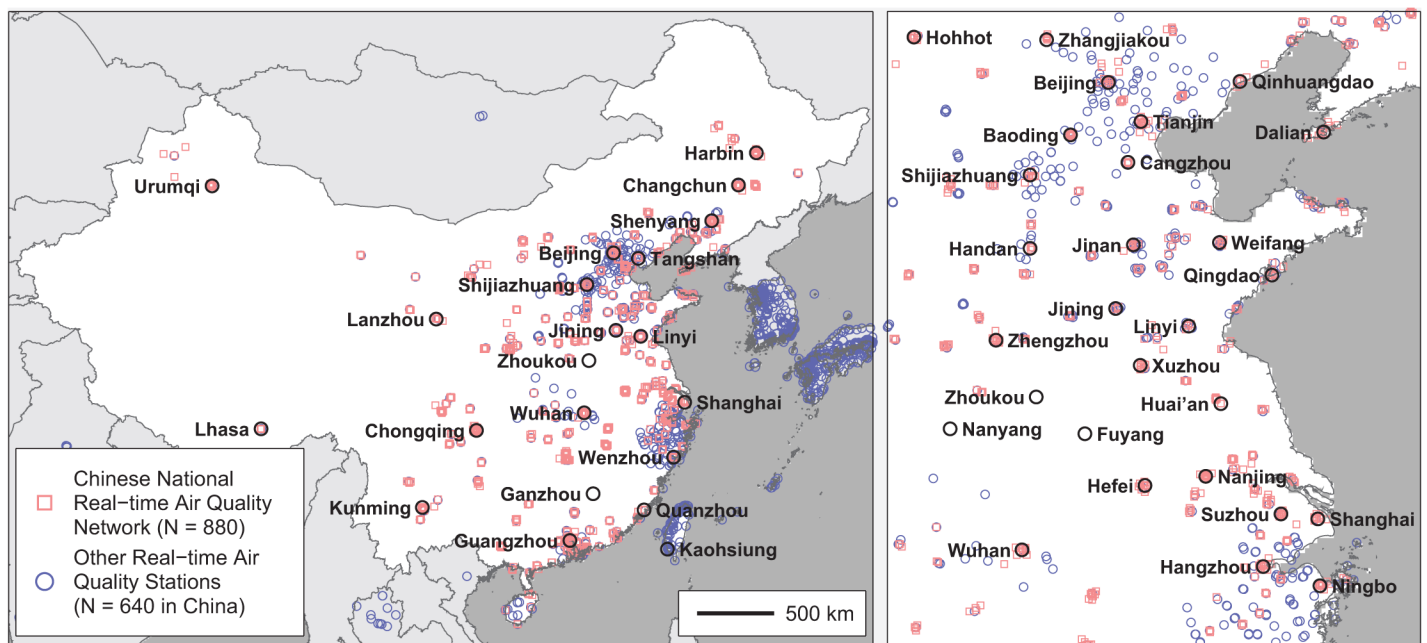
Fig 1. Map of real-time air pollution monitoring stations. Map shows the locations of air quality monitoring sites in China and surrounding areas with sufficient hourly data to be included in this study. Selection criteria and data sources are described in S1 Text. The map was prepared in MATLAB using political boundaries from the Global Database of Administrative Areas (version 2; http://gadm.org/).

doi:10.1371/journal.pone.0135749.g001

For each pollutant, a correlation vs. distance function was estimated by computing all possible pairwise correlations between different stations and fitting the resulting correlations to a two part exponential decay as a function of distance. The resulting functional forms are stated in S2 Table and shown in S2 and S3 Figs. The correlation functions are used to construct correlation matrices that in turn are used to compute Kriging coefficients [14, 15], $K_n(\vec{x})$.

The interpolated pollutant field, $P(\vec{x}, t)$, is then estimated in two parts.

$$P(\vec{x}, t) = S(\vec{x}) + A(\vec{x}, t)$$

$$S(\vec{x}) = \left(\sum_n K_n(\vec{x}) \left(\bar{p}_n - G(\vec{x}_n) \right) \right) + G(\vec{x})$$

$$A(\vec{x}, t) = \sum_n K_n^*(\vec{x}, t)(p_n(t) - \bar{p}_n)$$

The stationary part, $S(\vec{x})$, is derived by applying Kriging interpolation to the mean pollutant concentrations and a global predictor, $G(\vec{x}_n)$, that depends on latitude and longitude and contains free parameters that are adjusted to fit the observed means. The time-dependent anomaly part, $A(\vec{x}, t)$, depends only on the fluctuations at each station relative to the local mean, and its Kriging coefficients, $K_n^*(\vec{x}_n, t)$, are computed with restriction to stations that are active at time t. This two-step process reduces errors associated with stations that have intermittently missing data. This method is similar to that used by Berkeley Earth for its historical earth temperature analysis [16]. Since the correlation vs. distance function has been constructed with the correlation at zero distance obtaining a value less than one, the resulting interpolated fields will be smoother than the original data. This design was chosen for its ability to compensate for noise in the underlying station measurements. Additional details of the interpolation process are provided in the supplement methods (S1 Text).

For mapping and computation, this continuous field was sampled with an approximately 6 km resolution, though in practice, the characteristic size of resolvable features is often larger (e.g. 30 km) and varies with station density and noise.

A simple estimate of pollutant fluxes, $F(\vec{x}, t)$, was computed by comparing observed changes in the hourly pollutant concentration to the concentrations expected due to short-term wind transport $\vec{v}(\vec{x}, t)$ and an exponential decay with lifetime τ. Differences from the simple transport and decay model are assumed to represent source fluxes.

$$F(\vec{x}, t) = \frac{P(\vec{x} + \vec{v}(\vec{x}, t)\,\Delta t, t + \Delta t) - e^{-\Delta t/\tau}P(\vec{x}, t)}{2\Delta t} + \frac{P(\vec{x}, t) - e^{-\Delta t/\tau}P(\vec{x} - \vec{v}(\vec{x}, t)\,\Delta t, t - \Delta t)}{2\Delta t}$$

The near-surface (80 m) wind field from the Global Forecast System [17] was used for this calculation, and the effective pollutant lifetime was estimated as described in S1 Text and reported in S2 Table. Flux averages were computed by time-averaging the resulting field after excluding outlying values and cells affected by rain events as determined from Tropical Rainfall Measuring Mission data [18, 19].

The change in mortality due to $PM_{2.5}$ air pollution was calculated by adopting the integrated exposure response function approach [20] which considers relative risk of death for five disease classes (stroke, ischemic heart disease, lung cancer, chronic obstructive pulmonary disease, and lower respiratory infection) and which was adopted by World Health Organization (WHO) for the Global Burden of Disease study [21]. The model incorporates non-linear response versus concentration and provides an estimate of uncertainty. Relative risk was calculated at the
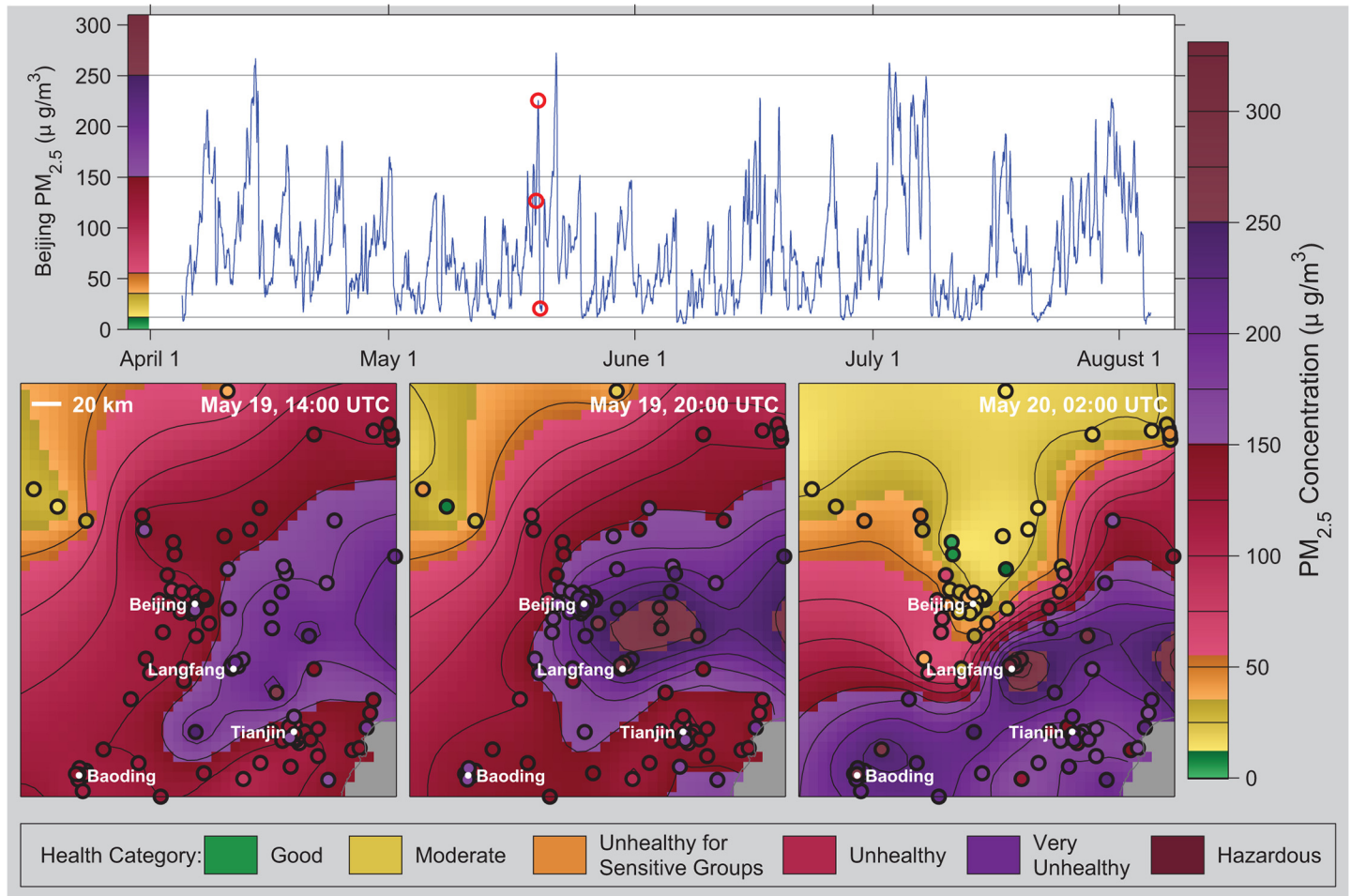
Fig 2. Time evolution of PM$_{2.5}$ pollution in the vicinity of Beijing. (Top) Time series of PM$_{2.5}$ concentration at Beijing extracted from the interpolated field. Red circles indicate times shown in bottom row. (Bottom) Maps of interpolated PM$_{2.5}$ concentration during a period of high pollution. Pollution concentrations were computed as described in the text from hourly data and maps were rendered in MATLAB. Concentrations are shown using color gradients and contour lines, where color tones (green, yellow, etc.) correspond to health impact categories defined by the US EPA. Bold circles show station locations with the observed value at each station indicated by the color within the circle.

doi:10.1371/journal.pone.0135749.g002

prefecture level using local average PM$_{2.5}$ concentration. The data for different diseases and prefectures was then combined to construct national average mortality estimates.

Analysis and figure rendering was performed using original software written for this project on the MATLAB platform (version 2014a; http://www.mathworks.com/). Additional details of these calculations and associated background information is provided in the supplemental methods document (S1 Text).

Results

Fig 2 shows a time series of PM$_{2.5}$ concentration at Beijing and interpolated maps at three time points separated by 6 hours each. This shows the volatile nature of air pollution and the role of weather patterns in redistributing pollution on short timescales. Our approach creates a smooth field that approximates the data at each station, but allows a degree of difference attributable to noise. The pollution is extensive and rapidly evolves in response to winds and other atmospheric conditions. In the figure, fresh air from the North displaces a period of heavy

pollution. Hourly data allows us to capture this evolution and ultimately estimate source fluxes. S1 Movie shows the time evolution of $PM_{2.5}$ across the entire country.

Fig 3 presents averages of the interpolated data for $PM_{2.5}$, PM_{10}, and O_3 across the study duration. The maps are color-coded based on US EPA health categories for 24-hour exposure [22]. Maps for SO_2 and NO_2 are included in the supplemental materials and show "good" levels nearly everywhere (S11 and S13 Figs).

Air pollution is extensive in China, with the highest particulate concentrations observed south of Beijing (e.g. Xingtai / Handan), but significant levels extend throughout the interior, which is consistent with previous satellite and modeling estimates [11–13]. Extensive pollution is not surprising since particulate matter can remain airborne for days to weeks and travel thousands of kilometers. The corridor south of Beijing contains the highest pollution concentrations and, as discussed below, many of the largest sources. During this study, the southern coastal area experienced somewhat better air quality, possibly linked to greater rainfall (S1 Fig).

For $PM_{2.5}$, portions of China encompassing roughly 38% of the population are classified as "unhealthy" on average (>55 $\mu g/m^3$, red) with an additional 45% of the population averaging "unhealthy for sensitive groups" (>35 $\mu g/m^3$, orange). Almost none of the study area averaged below the US EPA's 12 $\mu g/m^3$ standard for annual average $PM_{2.5}$ exposure (green). The area-weighted average was 46 $\mu g/m^3$ and the population-weighted average exposure to $PM_{2.5}$ was 52 $\mu g/m^3$. 92% of China's population experienced unhealthy $PM_{2.5}$ for at least 120 hours during the study period. 46% of China's population experienced $PM_{2.5}$ above the highest EPA threshold ("hazardous", >250 $\mu g/m^3$), during at least one hour in the observation period.

Patterns for PM_{10} are similar but less severe, with average PM_{10} levels "moderate" for most of China. Ozone concentrations are modest across most of China, though higher levels occur in the Northwest desert area, and in a small number of Northeastern cities. Though the average levels of PM_{10} and O_3 are "moderate" or "good" for much of China, intermittently high levels of these pollutants can occur in some areas.

Source Regions for Air Pollution in China

Fig 4 shows estimated pollutant fluxes for $PM_{2.5}$, PM_{10}, SO_2, and NO_2. Pollution emission is often localized, especially in the Beijing to Shanghai corridor where many of the highest PM concentrations also occur (Fig 3). Most of the largest emissions appear in or near urban areas (e.g. Handan, Shijazhuang, Zibo, Tangshan, Linyi, Hangshou), though not all major cities have high pollution fluxes (e.g. Chongqing, Chengdu, Wuhan). The source map presumably reflects patterns of industrial activity, though detailed differences will not be explored here.

NO_2 and SO_2 emissions help suggest the pollution source. Nitrogen oxides, including nitric oxide (NO) and NO_2 are created when air is heated, and on average have been attributed to transportation fuels (15–25%), fossil fuel burning in power plants (30–50%), and to industrial facilities (25–35%) [23, 24]. It is expected that NO dominates at the combustion source, but in the presence of sunlight NO and NO_2 will equilibrate within a few minutes (as well as reacting with O_3), implying that NO_2 measurements reflect a combination of NO and NO_2 emissions. SO_2 emissions have been previously associated with coal (~90%) in power plants and industrial facilities [25]. Beijing has negligible SO_2 flux, despite a large NO_2 signal, possibly a result of policies that limit coal burning in the immediate vicinity of Beijing and more extensively apply mitigation technologies.

Many of the SO_2 and NO_2 sources are also sources of PM pollution. This is not surprising since fossil fuel burning is also a major source of $PM_{2.5}$ and PM_{10}. However, the PM sources appear more diffuse than either the SO_2 or NO_2 sources. In part, this is caused by secondary particulate matter formed within the atmosphere from other pollutants, such as SO_2 or NO_2
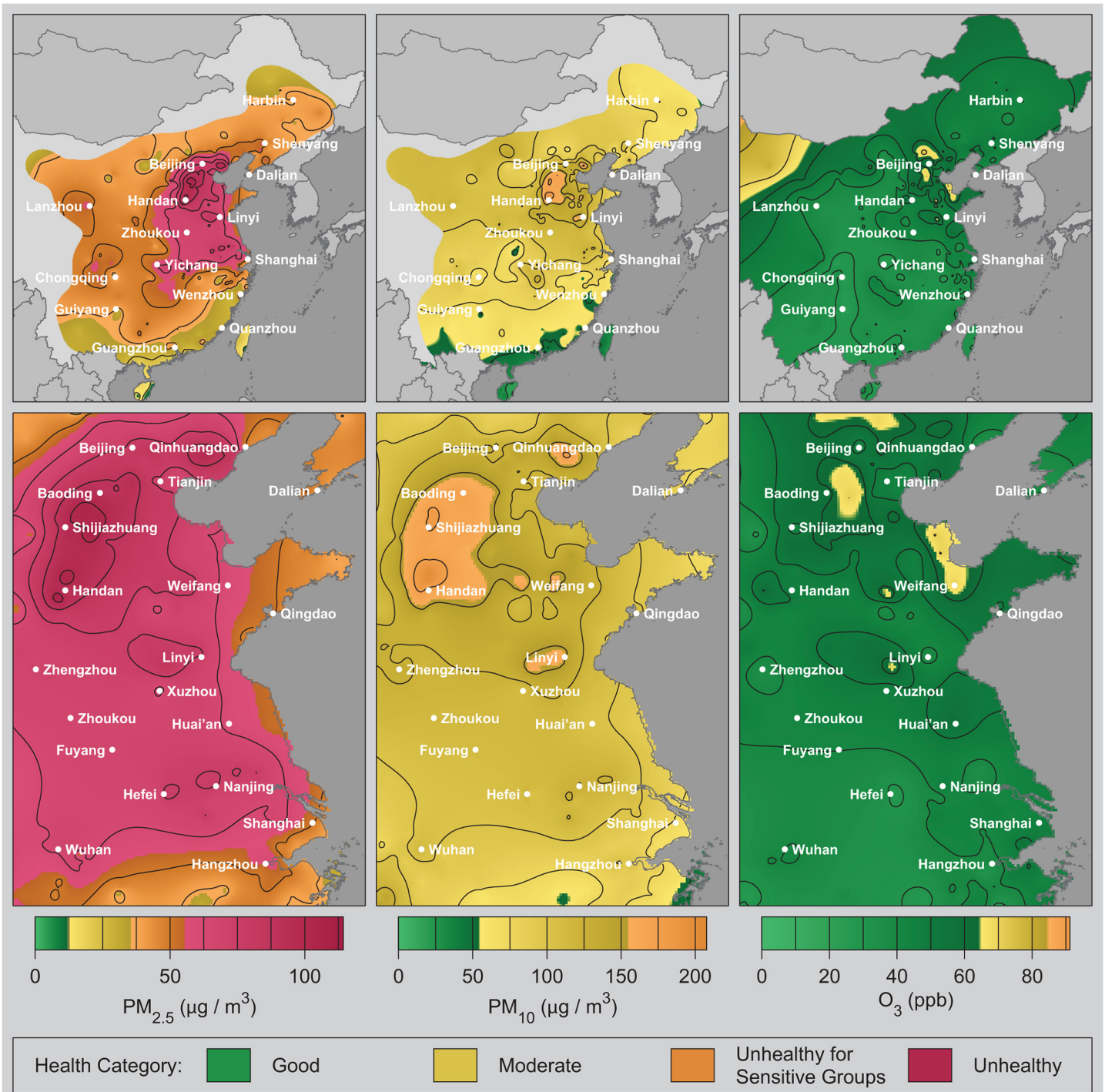
Fig 3. Average air pollution maps. Maps of average pollutant concentration for PM$_{2.5}$, PM$_{10}$, and O$_3$ for eastern China (top row) and the Beijing to Shanghai corridor (bottom row). Concentrations are shown using color gradients and contour lines; the colors (green, yellow, etc.) represent US EPA qualitative health impacts. Pollution concentrations were computed as described in the text using hourly data and then the hourly concentration fields were averaged over the four month study duration. The resulting maps were rendered using MATLAB.

[26]. Secondary particulate formation may cause PM fluxes to appear more widely distributed than the underlying emitters. Nonetheless, many strong PM sources are identified through this
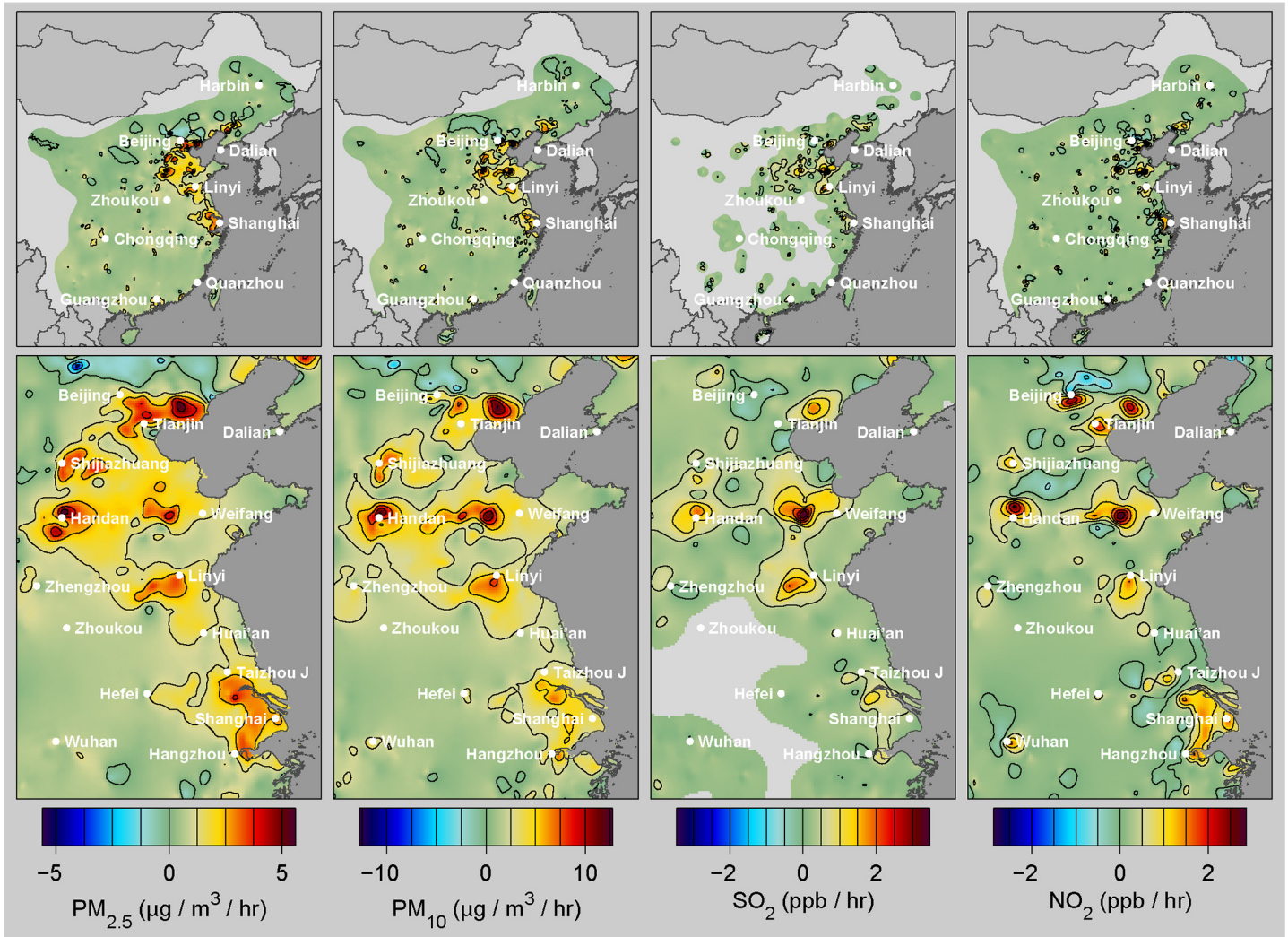
Fig 4. Air pollution source maps. Maps of average pollutant flux for PM$_{2.5}$, PM$_{10}$, SO$_2$, and NO$_2$ for eastern China (top row) and the Beijing to Shanghai corridor (bottom row). Pollutant fluxes were computed as described in the text from changes in the interpolated hourly pollution fields along with contemporaneous wind and weather data. Due to sparse sampling and secondary transformations of pollutants in the atmosphere, apparent source fluxes are likely to appear more diffuse than the true emissions source.

doi:10.1371/journal.pone.0135749.g004

analysis. Within the study region, 10% of the area is responsible for 34% of the PM$_{2.5}$ emissions, and 5% of the area is responsible for 22% of emissions. However, small and moderate sources are also important. Approximately 37% of the study region had PM$_{2.5}$ fluxes >0.5 μg/m^3/hr, sufficient to exceed US EPA standards after only 3 days of stagnant air.

Discussion

We have presented a technique for mapping air pollution concentrations and sources using data from monitoring stations. As has been known from satellite and modeling studies, particulate pollution is an extensive problem affecting nearly all of China's population, but the observed heterogeneity of source locations could help develop strategies to reduce pollution.

We examined a four month interval as long-term station data were not available for most of China. Previous studies of both in situ and satellite data have indicated that winter and early spring months in China have somewhat higher PM concentrations due to increased use of

fossil fuels for seasonal heating, weather patterns that concentrate pollution at low altitudes, and increased desert dust fluxes [12, 27]. In contrast, the air in China is typically cleanest from late summer to early fall. The April 5 to August 5 study period is somewhat intermediate. A review of hourly $PM_{2.5}$ station data from Beijing (2009–2014), Shanghai (2012–2014), Guangzhou (2012–2014), Chengdu (2013–2014), and Shenyang (2014) indicates that the months studied in this paper averaged 91%, 84%, 89%, 72%, and 73% respectively of the annual averages (U.S. Air Quality Monitoring Program, http://www.stateair.net/web/mission/1/). Monthly-resolved $PM_{2.5}$ satellite data for the whole study region was not immediately available, but a monthly satellite history for Beijing reported that April-July averaged 99% of the annual mean during 2000 to 2012 [28]. Hence, particulate pollution estimates drawn from the current short study period will likely be similar to or somewhat lower than long-term averages. Future work could explore seasonal variations and long-term trends.

During the four months studied, the population-weighted and area-weighted $PM_{2.5}$ averages were 52 and 46 μg/m^3 respectively. Satellite pollution datasets generally focus on annual or multi-year averages, which limits the ability to make direct comparisons. However, the available satellite estimates tend to be similar to or somewhat lower than the ground observations. An analysis of the larger East Asia region estimated a population-weighted $PM_{2.5}$ exposure of 50 μg/m^3 for 2001 to 2010 [28]. A version of the same dataset masked to the current study region had an area-weighted average of 40 μg/m^3 from 2010 to 2012 [28, 29]. A different satellite estimate using similar observations but different calibrations and modeling gave 25 μg/m^3 for the 2008 to 2010 average over the present study region [30, 31]. Both of these datasets show similar spatial patterns to what we observe (Fig 5), though the magnitudes in van Donkelaar et al.'s work [28] are clearly more consistent with our ground data estimates. As noted in previous satellite to in situ comparisons, satellite data may be more likely to underestimate pollution concentrations during the most extreme pollution events [28, 32].

The conversion of pollution concentrations to mortality is complicated. We adopt the framework [20] developed for the WHO Global Burden of Disease study [21] that considers $PM_{2.5}$ mortality due to impacts on five distinct diseases and accounts for nonlinearities as a function of concentration. Using prefecture level population and pollution data along with national average death rates for the five modeled diseases, we calculate that 1.6 million deaths / year can be attributed to $PM_{2.5}$ air pollution under the WHO model [95% confidence: 0.7 to 2.2 million deaths/year]. This is equivalent to 4 thousand deaths / day or 17% of all deaths in China. Additional details appear in S1 Text and S1 Table. For perspective, the categories of mortality events considered by the WHO model, e.g. cardiorespiratory deaths, account for roughly 55% of all Chinese deaths [21]. This compares to only 42% of mortality in the United States in the same cardiorespiratory categories, despite much higher incidence of obesity in the United States [21]. The calculated mortality is somewhat higher than the 1.2 million deaths/year previously estimated from the Huai River study using Chinese air pollution measurements and mortality data [3,4,33].

Though most of China is subject to potentially harmful levels of $PM_{2.5}$, some large population centers (Chongqing, Wuhan, Chengdu) emit less than half the $PM_{2.5}$ of others. Among northeastern cities, Beijing has relatively low emissions except for NO_2. Low SO_2 fluxes may indicate cities that benefit from lower coal usage or better smokestack pollution controls. Compared to natural gas, coal produces 150 to 400 times more PM for the same energy delivered [34,35]. China has plans for new coal plants in the next decade that could effectively double their coal consumption [36], potentially exacerbating the problem of air pollution. A table of pollution concentrations and fluxes by province and prefecture is included in S1 Table.

The methods of this study should be applicable to air quality monitoring in other regions of the world. However, these techniques require an extensive air-quality monitoring network with frequent updates (e.g. hourly), and such networks presently exist in only a few places. We hope
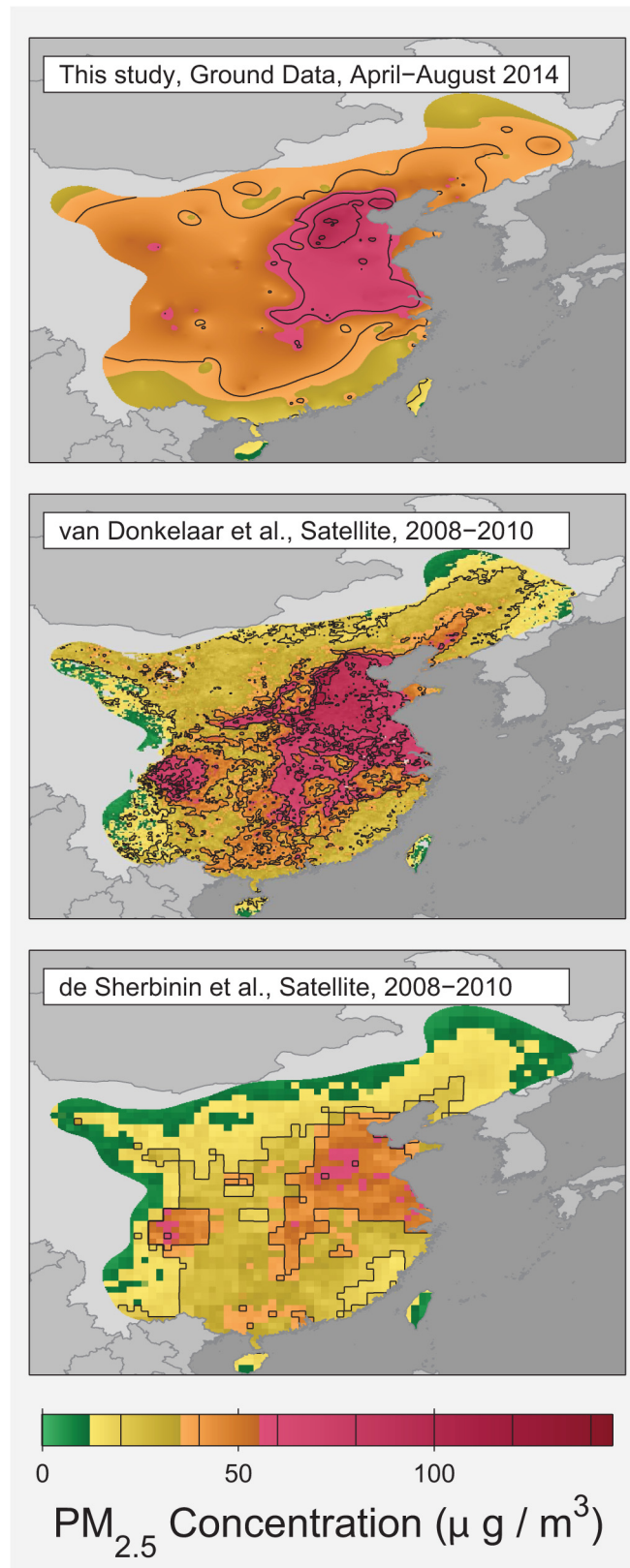
Fig 5. Comparison of PM₂.₅ observations to satellite data. Maps of average PM$_{2.5}$ concentration from this study (top) and two satellite-derived datasets restricted to the same region. The average over the 2008 to

2010 time interval was chosen for the satellite data due to the limitations of the available satellite data. Both the concentrations reported by van Donkelaar [28] (middle) and those reported by de Sherbinin [30] (bottom) rely on similar satellite observations of aerosol optical depth (obtained by NASA), but interpret those observations differently when determining pollutant concentration. The satellite-derived data was imported from concentration data files provided by their respected sources and rendered via MATLAB to use the same US EPA health category color scheme applied in Figs 2 and 3.

doi:10.1371/journal.pone.0135749.g005

that other countries will follow China's lead and provide both extensive and transparent real-time air quality monitoring.

Supporting Information

S1 Text. Supplemental Methods. Additional discussion of methods, data handling, and validation.
(DOCX)

S1 Table. Province and prefecture pollution and mortality data. Provides pollution concentration and flux data broken down by geographic regions within China. Also provides the details of the associated mortality calculation.
(XLSX)

S2 Table. Correlation vs. distance and lifetime of air pollutants in China. Summary of the empirically determined correlation vs. distance functions for the five pollutants discussed in this study and the effective residence time in the atmosphere of their pollutant plumes in the absence of rain or snow. The correlation functions generally consist of a short range component (influenced largely by source distributions) and a long-range component (influenced by weather patterns). The effective pollutant plume lifetime shows the value empirically estimated for this study. Ranges in brackets indicate alternative lifetimes making different assumptions as discussed in the Supplemental Methods (S1 Text).
(DOCX)

S1 Movie. Animation of PM$_{2.5}$ Concentrations. Movie showing the evolution of PM$_{2.5}$ concentrations, as inferred by this study, across Eastern China during the four month study interval. Concentrations are shown using color gradients and contour lines; the colors (green, yellow, etc.) represent US EPA qualitative health impacts based on 24-hour exposure. Green is "Good", yellow is "Moderate", orange is "Unhealthy for Sensitive Groups", red is "Unhealthy", purple is "Very Unhealthy", and dark red is "Hazardous". Concentrations higher than the upper limit of the maximum EPA classification are shown in gray.
(MP4)

S1 Fig. Average wind and rain patterns in Eastern China. (Left) Average wind speed pattern across China and surrounding areas during the period of this study according to Global Forecast System data at 80 m altitude. Arrow lengths are proportional to wind speed and the legend indicates the size of arrow consistent with a 10 km/hr average wind speed. (Right) Percentage of hours for each grid cell where rain was experienced during the study period based on observations from the Tropical Rainfall Measurement Mission satellite data. Maps were prepared with MATLAB with political boundaries from the Database of Global Administrative Areas (GADM version 2).
(TIF)

S2 Fig. Pollution concentration correlation vs. distance. Summary of empirically estimated correlation vs. distance functions for the five pollutants studied. Same values as S2 Table.
(EPS)

S3 Fig. Empirical fit of PM$_{2.5}$ correlation data. Heat map of correlation vs. distance generated by all possible pairwise comparisons of PM$_{2.5}$ data from stations in this study. Brighter colors indicate more frequently occurring combinations of R-value and distance, and are normalized for the abundance of comparisons at each distance. The red curve indicates the correlation vs. distance model fit to this data and described in S2 Table.
(EPS)

S4 Fig. Impact of assumed plume lifetime on PM$_{2.5}$ source distribution. Maps comparing calculated PM$_{2.5}$ source fluxes for different assumed values of the effective plume lifetime. The upper right panel corresponds to the data reported in the main paper, and has a lifetime chosen such that 5% of the field area is allowed to be negative (same as Fig 4 and S8 Fig). The upper left panel, corresponds to choosing a decay lifetime such that 2% of the flux field is negative, the lower left panel has 15% negative area, and the lower right panel has no plume decay in the absence of rain (infinite lifetime). Rain events are explicitly excluded from consideration, and the reported flux aims to capture the man-made sources of pollution. In general, assuming a shorter plume lifetime implies higher and more diffuse fluxes in order to maintain the observed concentration patterns. By contrast, if the pollutant plumes are assumed to have a very long lifetime then the apparent man-made flux will implausibly turn negative over substantial regions. Though quantitatively important, the choice of effective lifetime has little qualitative impact on the distribution of large sources. The regions of locally higher flux remain similar under all scenarios.
(TIF)

S5 Fig. Comparison of PM$_{2.5}$ patterns in early and late half of study. Maps comparing PM$_{2.5}$ concentrations (top) and fluxes (bottom) during the first half of the sampling period (left column) and the second half of the sampling period (right). PM$_{2.5}$ concentrations are presented using the same health impact associated color scheme as Fig 3.
(TIF)

S6 Fig. Comparison of PM$_{2.5}$ patterns from half-density reconstructions. The collection of available stations was randomly assigned to two groups, and the analyses for PM$_{2.5}$ concentrations (top) and fluxes (bottom) were repeated in full for both groups. These independent sub-samples result in similar concentration and flux patterns, implying the reconstructions are likely to be stable with respect to data selection.
(TIF)

S7 Fig. Average PM$_{2.5}$ concentration across China. Larger version of panel from Fig 3 presenting PM$_{2.5}$ concentrations across China. Concentrations are shown using color gradients and contour lines; the colors (green, yellow, etc.) represent US EPA qualitative health impacts. Based on 24-hour exposure green is "Good", yellow is "Moderate", orange is "Unhealthy for Sensitive Groups" and red is "Unhealthy".
(EPS)

S8 Fig. PM$_{2.5}$ sources across China. Larger version of panel from Fig 4 presenting PM$_{2.5}$ source fluxes across China.
(EPS)

S9 Fig. Average PM$_{10}$ concentration across China. Larger version of panel from Fig 3 presenting PM$_{10}$ concentrations across China. Concentrations are shown using color gradients and contour lines; the colors (green, yellow, etc.) represent US EPA qualitative health impacts. Based on 24-hour exposure green is "Good", yellow is "Moderate", orange is "Unhealthy for

Sensitive Groups" and red is "Unhealthy".
(EPS)

S10 Fig. PM$_{10}$ sources across China. Larger version of panel from [Fig 4](#) presenting PM$_{10}$ source fluxes across China.
(EPS)

S11 Fig. Average SO$_2$ concentration across China. Map of SO$_2$ concentrations across China. Concentrations are shown using color gradients and contour lines; the colors (green, yellow, etc.) represent US EPA qualitative health impacts. Based on 24-hour exposure green is "Good", yellow is "Moderate", orange is "Unhealthy for Sensitive Groups" and red is "Unhealthy". The limited coverage of this map is a consequence of the short correlation length for SO$_2$ ([S2 Table](#); [S2 Fig](#)), which limits the distance over which one can usefully interpolate SO$_2$. In part, the short correlation length is a consequence of the short lifetime of SO$_2$ in the atmosphere, which makes estimates far from measurement sites highly uncertain.
(EPS)

S12 Fig. SO$_2$ sources across China. Larger version of panel from [Fig 4](#) presenting SO$_2$ source fluxes across China.
(EPS)

S13 Fig. Average NO$_2$ concentration across China. Map of NO$_2$ concentrations across China. Concentrations are shown using color gradients and contour lines; the colors (green, yellow, etc.) represent US EPA qualitative health impacts. Based on 24-hour exposure green is "Good", yellow is "Moderate", orange is "Unhealthy for Sensitive Groups" and red is "Unhealthy".
(EPS)

S14 Fig. NO$_2$ sources across China. Larger version of panel from [Fig 4](#) presenting NO$_2$ source fluxes across China.
(EPS)

S15 Fig. Average O$_3$ concentration across China. Larger version of panel from [Fig 3](#) presenting O$_3$ concentrations across China. Concentrations are shown using color gradients and contour lines; the colors (green, yellow, etc.) represent US EPA qualitative health impacts. Based on 24-hour exposure green is "Good", yellow is "Moderate", orange is "Unhealthy for Sensitive Groups" and red is "Unhealthy".
(EPS)

S16 Fig. O$_3$ sources across China. Map of O$_3$ source fluxes across China.
(EPS)

Acknowledgments

Author Contributions

Conceived and designed the experiments: RAM RAR. Performed the experiments: RAR. Analyzed the data: RAR RAM. Contributed reagents/materials/analysis tools: RAR. Wrote the paper: RAM RAR.

References

1. World Health Organization. WHO methods and data sources for global causes of death 2000–2012. Global Health Estimates Technical Paper WHO/HIS/HSI/GHE/2014.7. 2014. Available: http://www.who.int/entity/healthinfo/global_burden_disease/GlobalCOD_method_2000_2012.pdf.

2. World Health Organization. Burden of disease from the joint effects of Household and Ambient Air Pollution for 2012. WHO Technical Report. 2012. Available: http://www.who.int/phe/health_topics/outdoorair/databases/AP_jointeffect_BoD_results_March2014.pdf.

3. O'Keefe B. Recent Trends in Air Quality Standards in Europe and Asia: What's next? HEI Annual Conference 2012. 2013. Available: http://www.healtheffects.org/Slides/AnnConf2013/OKeefe-Sun.pdf.

4. Yang G, Wang Y, Zeng Y, Gao GF, Liang X, Zhou M, et al. Rapid health transition in China, 1990–2010: findings from the Global Burden of Disease Study 2010. Lancet 2013; 381: 1987–2015. doi: 10.1016/S0140-6736(13)61097-1 PMID: 23746901

5. Dockery DW, Pope CA, Xu X, Spengler JD, Ware JH, Fay ME, et al. An association between air pollution and mortality in six U.S. cities. N Engl J Med 1993; 329(24), 1753–1759. PMID: 8179653

6. Pope CA, Burnett RT, Thun MJ, Calle EE, Krewski D, Ito K, et al. Lung cancer, cardiopulmonary mortality, and long-term exposure to fine particulate air pollution. JAMA 2002; 287(9): 1132–1141. doi: 10.1001/jama.287.9.1132 PMID: 11879110.

7. Hoek G, Krishnan RM, Beelen R, Peters A, Ostro B, Brunekreef B, et al. Long-term air pollution exposure and cardiorespiratory mortality: a review. Env Health. 2012; 12:43.

8. Beelen R, Raaschou-Nielsen O, Stafoggia M, Andersen ZJ, Weinmayr G. Effects of long-term exposure to air pollution on natural-cause mortality: an analysis of 22 European cohorts within the multicentre ESCAPE project. Lancet 2013; 383(9919): 785–795. doi: 10.1016/S0140-6736(13)62158-3 PMID: 24332274

9. Government of China. Ambient Air Quality Standards (in Chinese). GB 3095–2012. 2012. Available: http://kjs.mep.gov.cn/hjbhbz/bzwb/dqhjbh/dqhjzlbz/201203/W020120410330232398521.pdf.

10. Zhang Q, Geng GN, Wang SW, Richter A, He KB. Satellite remote sensing of changes in NO_x emissions over China during 1996–2010. Chinese Sci. Bull. 2012; 57(22): 2857–2864. doi: 10.1007/s11434-012-5015-4

11. Wang J, Xua X, Spurr R, Wang Y, Drury E. Improved algorithm for MODIS satellite retrievals of aerosol optical thickness over land in dusty atmosphere: Implications for air quality monitoring in China. Remote Sensing Env. 2010; 114: 2575–2583.

12. Liu X-H, Zhang Y, Cheng S-H, Xing J, Zhang Q, Streets DG, et al. Understanding of regional air pollution over China using CMAQ, part I: performance evaluation and seasonal variation. Atmos Env. 2010; 44(20): 2415–2426.

13. Lei Y, Zhang Q, He K, Streets D. Primary anthropogenic aerosol emission trends for China, 1990–2005. Atmos Chem Phys. 2011; 11, 931–954.

14. Schabenberger O, Gotway CA. Statistical Methods for Spatial Data Analysis. CRC Press. 2004.

15. Krige DG. A statistical approach to some basic mine valuation problems on the Witwatersrand. J Chem Metall Min Soc S Afr. 1951; December: 119–159.

16. Rohde RA, Muller RA, Jacobsen R, Perlmutter S, Rosenfeld A, Wurtele J., et al. Berkeley Earth Temperature Averaging Process. Geoinfor Geostat: An Overview 2013; 1(2) doi: 10.4172/gigs.1000103

17. NOAA/NCEP. Global Forecast System (GFS) Atmospheric Model. 2012. Available: www.ncdc.noaa.gov/data-access/model-data/model-datasets/global-forcast-system-gfs

18. Huffman GJ, Adler RF, Bolvin DT, Gu G, Nelkin EJ, Bowman KP, et al. The TRMM Multi-satellite Precipitation Analysis: Quasi-global, multi-year, combined-sensor precipitation estimates at fine scale. J. Hydrometeor. 2007; 8(1): 38–55.

19. Huffman GJ, Bolvin DT. Real-Time TRMM Multi-Satellite Precipitation Analysis Data Set Documentation. NASA/GSFC Laboratory for Atmospheres, 43 pp. 2011. Available: ftp://meso.gsfc.nasa.gov/pub/trmmdocs/rt/3B4XRT_doc.pdf.

20. Burnett RT, Pope CA III, Ezzati M, Olives C, Lim SS, Mehta S, et al. An integrated risk function for estimating the global burden of disease attributable to ambient fine particulate matter exposure. Env Health Perspect 2014; 122:397–403. doi: 10.1289/ehp.1307049

21. Naghavi M, Wang H, Lozano R, Davis A, Liang X, Zhou M, et al. Global, regional, and national age–sex specific all-cause and cause-specific mortality for 240 causes of death, 1990–2013: a systematic analysis for the Global Burden of Disease Study 2013. Lancet 2015; 385 (9963): 117–171. doi: 10.1016/S0140-6736(14)61682-2 PMID: 25530442

22. US EPA. Air Quality Index: A Guide to Air Quality and Your Health. U.S. EPA Report EPA-456/F-14-002. 2014. Available: http://www.epa.gov/airnow/aqi_brochure_02_14.pdf.

23. Emission Database for Global Atmospheric Research (EDGAR), release 4.2. Available: http://edgar.jrc. ec.europa.eu.

24. Shi Y, Xia Y-F, Lu B, Liu N, Zhang L, Li S-J, et al. Emission inventory and trends of NO_x for China, 2000–2020. J Zhejiang Univ-SCI A 2014; 15(6):454–464.

25. Lu Z, Zhang Q, Streets D. Sulfur dioxide and primary carbonaceous aerosol emissions in China and India, 1996–2010. Atmos Chem Phys. 2011; 11: 9839–9864.

26. Davidson C, Phalen R, Solomon P. Airborne particular matter and human health: a review. Aerosol Sci Technol. 2005; 39: 737–749.

27. Zhang W-J, Sun Y-L, Zhuang G-S, Xu D-Q. Characteristics and Seasonal Variations of PM2.5, PM10, and TSP Aerosol in Beijing. Biomed Env Sci 2006; 19: 461–468.

28. van Donkelaar A, Martin RV, Brauer M, Boys BL. Global fine particulate matter concentrations from satellite for long-term exposure assessment. Env Health Perspectives 2015. doi: 10.1289/ehp.1408646

29. Boys BL, Martin RV, van Donkelaar A, MacDonell R., Hsu NC, Cooper MJ, Yantosca RM, Lu Z, Streets DG, Zhang Q, Wang S. Fifteen-year global time series of satellite-derived fine particulate matter, Env Sci Technol. 2014. doi: 10.1021/es502113p

30. de Sherbinin A, Levy M, Zell E, Weber S, Jaiteh M. Using Satellite Data to Develop Environmental Indicators. Environmental Research Letters 2014; 9(8): 084013. doi: 10.1088/1748-9326/9/8/084013

31. Battelle Memorial Institute, Center for International Earth Science Information Network—CIESIN—Columbia University. Global Annual Average PM2.5 Grids from MODIS and MISR Aerosol Optical Depth (AOD). Palisades, NY: NASA Socioeconomic Data and Applications Center (SEDAC). 2013. doi: 10.7927/H4H41PB4

32. Song W, Jia H, Huang J, Zhang Y. A satellite-based geographically weighted regression model for regional PM2.5 estimation over the Pearl River Delta region in China. Remote Sensing Env. 2014; 154: 1–7.

33. Chen Y, Ebenstein A, Greenstone M, Lie H. Evidence on the impact of sustained exposure to air pollution on life expectancy from China's Huai River policy. PNAS 2013; 110(32): 12936–12941. doi: 10.1073/pnas.1300018110 PMID: 23836630

34. Cai H, Wang M, Elgowainy A, Han J. Updated Greenhouse Gas and Criteria Air Pollutant Emission Factors and Their Probability Distribution Functions for Electric Generating Units. Argonne National Laboratory ANL/ESD/12-2. 2012.

35. US Energy Information Agency. Natural Gas 1998, Issues and Trends. US EIA Report DOE/EIA-0560 (98). 1998. Available: http://www.eia.doe.gov/oil_gas/natural_gas/analysis_publications/natural_gas_ 1998_issues_and_trends/it98.html.

36. Yang A, Cui Y. Global Coal Risk Assessment: Data Analysis and Market Research. World Resources Institute Working Paper. 2012. Available: http://pdf.wri.org/global_coal_risk_assessment.pdf.